Ion-Specific Induced Charges at Aqueous Soft Interfaces

Wenjie Wang, Rebecca Y. Park, Alex Travesset, and David Vaknin

Ames Laboratory, and Department of Physics and Astronomy, Iowa State University, Ames, Iowa 50011, USA

(Received 8 September 2010; revised manuscript received 29 November 2010; published 2 February 2011)

Ionic specificity effects, i.e., ions of the same valence leading to different macroscopic effects, are studied by considering a Langmuir monolayer of arachidic acid over a solution containing either Fe^{3+} or La^{3+}. We systematically vary pH levels as a way to control the interfacial surface charge and characterize the system by surface-sensitive x-ray scattering and spectroscopic techniques. We show that the critical surface pressure at the tilted ($L2$) to untilted (LS) transition is ionic specific and varies with pH. While the maximum density of surface bound La^{3+} per head group of arachidic acid is ~ 0.3, the amount necessary to neutralize the surface charge, for Fe^{3+} it is nearly 0.6 and it is accompanied with a significant accumulation of the coions Cl^- as revealed by surface x-ray spectroscopy. We account for the experimental observations by a statistical mechanical model including ion specificity.

DOI: 10.1103/PhysRevLett.106.056102 PACS numbers: 82.45.Mp

It is often observed in aqueous media that different ions of the same valence give rise to dramatically different phases or charge distributions [1–7]. This ionic specificity arises because, in addition to long-range electrostatic interactions, short-range interactions, quantum mechanical in origin and highly specific to the ion and the interfacial charged group, are in play and need to be considered. In fact, accounting for both interactions in theoretical models is still a hurdle in the process towards a comprehensive understanding of soft matter electrostatics.

In this study, a monolayer of densely packed carboxyl groups in contact with solutions containing the trivalent ions Fe^{3+} and La^{3+} are considered, where the surface charge is regulated externally by deprotonation of the carboxyl group by varying pH levels. While the electronic configuration of Fe^{3+} allows for strong ion-specific interactions, both with carboxyl and water hydroxyl groups, La^{3+} is a good candidate of a ''classical'' trivalent ion for which long-range electrostatic interactions dominate.

Considering phase transitions of monolayers (for instance, $L2$-LS of fatty acids), under various subphase conditions, allows characterization of the complex effects of ions and pH on the amphiphiles. We thus express the critical external pressure π_c at the transition as

$$\pi_c = \pi_c^0 + \delta\pi_c, \tag{1}$$

where π_c^0 is the critical external pressure at zero ionic strength (and $p\mathrm{H} < pK_a$). The relevant observation is that $\delta\pi_c$ arises exclusively from changes at the headgroup by subphase properties such as ionic strength or pH. Physically, $\delta\pi_c$ is the extra surface-pressure reduction (or increase) induced by the attractive (or repulsive) forces exerted by charges at the headgroup region. Recent studies at the LE-$L2$ transition [8] have shown that while $\delta\pi_c$ is strongly dependent on ionic specificity, both the tilt angle and the compressibility are the same at the transition, in complete agreement with Eq. (1) and our approach.

Ion bulk concentrations were prepared using solutions of $FeCl_3$ and $LaCl_3$, obtained from Sigma-Aldrich. Ultrapure water (Millipore, Milli-Q, and NANOpure, Barnstead; resistivity, 18.1 MΩ cm) was used for all subphase preparations, and HCl solution was used to adjust pH. Arachidic acid (AA, $C_{20}H_{40}O_2$, CAS No. 506-30-9) was purchased from Sigma Chemical Co. Pure AA was dissolved in 3:1 chloroform-methanol solution and spread at gas-water interfaces in a thermostatic, Teflon Langmuir trough kept at 20 °C. Compression of monolayers, at a rate of ~ 1 Å^2 per molecule per minute, was started 10–15 min after spreading to allow for solvent evaporation, and surface pressure was recorded with a microbalance using a Wilhelmy paper plate. X-ray scattering studies were conducted on the Ames Laboratory Liquid Surface Diffractometer at the Advanced Photon Source (APS, 8.0 keV; $\lambda = 1.5498$ Å), beam line 6ID-B (described elsewhere [9]), and on a similar in-house liquid reflectometer using the UltraX-18 Rigaku generator as the x-ray source (Cu-K_α). X-ray reflectivity (XR) as a function of Q_z ($Q_z = 4\pi \sin\alpha_i/\lambda$, α_i being x-ray incident angle with respect to the interface) was used to yield the electron density (ED) profile normal to the interface [7]. X-ray fluorescence from the films using a Vortex energy dispersive detector was used to determine quantitatively the density of specific ions that accumulate at the interface [10].

Figures 1(a) and 1(b) show a few surface-pressure (π) versus molecular area isotherms ($T \approx 20°$) for arachidic acid that are spread on $FeCl_3$ and $LaCl_3$ solutions ($10^{-3}M$) at various pH values as indicated. It is clear that the isotherms are modified in the presence of ions and are strongly pH dependent. Above a certain pH the critical pressure π_c (the signature of tilted-untilted transition) cannot be identified, and as the pH decreases π_c increases so that below a certain pH the isotherm behaves as if the AA was spread on pure water with no ions in the solution. It is also evident that the effect of pH on the isotherms is

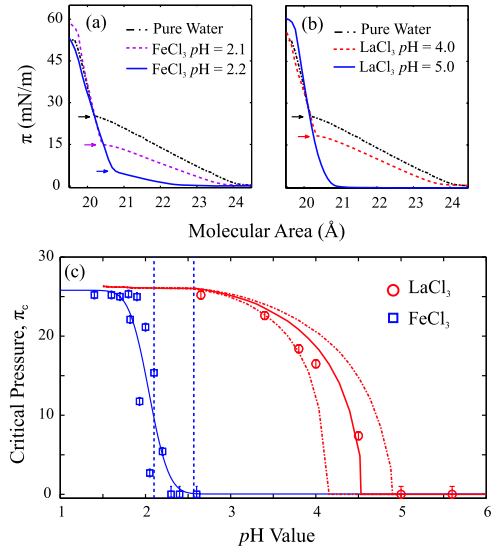

FIG. 1 (color online). Isotherms of AA on pure water and on (a) $FeCl_3$ of $10^{-3}M$ and (b) $LaCl_3$ of $10^{-3}M$ solutions at various pH values (arrows indicate π_c). (c) L-S critical surface pressure π_c as a function of pH for Fe^{3+} and La^{3+}. The solid line for La^{3+} is calculated with Eq. (2) and the dashed curves provide the limiting cases with reasonable variations of parameters used in the theoretical model. The two vertical dashed lines indicate the pH_c (left) and pH_M (right) (solid line for $FeCl_3$ data is for display only).

different for Fe^{3+} and La^{3+}. In Fig. 1(c) we compile all π_c values versus pH for the two solutions, showing the strong ion-specific differences. A notable difference is the range over which π_c varies (from 0 to its maximum value), nearly 2 pH units for La^{3+} compared to a few tenths for Fe^{3+}. Also the onset of the changes in π_c for La^{3+} nearly coincides with the pK_a value (~ 5.1) for AA but far from this value for Fe^{3+}.

These results are corroborated by the x-ray studies that furthermore provide quantitative information on ion binding. XR normalized to the calculated reflectivity of an ideally flat water surface (R/R_F) are shown in Fig. 2(a). The solid lines are the best-fit model calculations obtained from the electron density profiles across the interface shown in Fig. 2(b). We note that the measured XR on pure water and on iron solution at $p\mathrm{H} = 1.5$ are within error the same, and produce the same electron density compared to the dramatic enhancement in the ED at the headgroup region at higher pH values. This strongly indicates that no Fe^{3+} ($10^{-3}M$) binding occurs at low pH values ($p\mathrm{H} \lesssim 1.5$). This is consistent with the fact that the isotherms on water and at $p\mathrm{H} = 1.5$ are practically the same, as mentioned above. From the analysis of the XR data, using space-filling models [7,11,12], we obtain the average number of bound ions per AA, molecular area, and chain-tilt angle (see supplemental material [13]). Similar XR measurements for La^{3+} solutions show similar trends but shifted in pH values in accordance with Fig. 1(c).

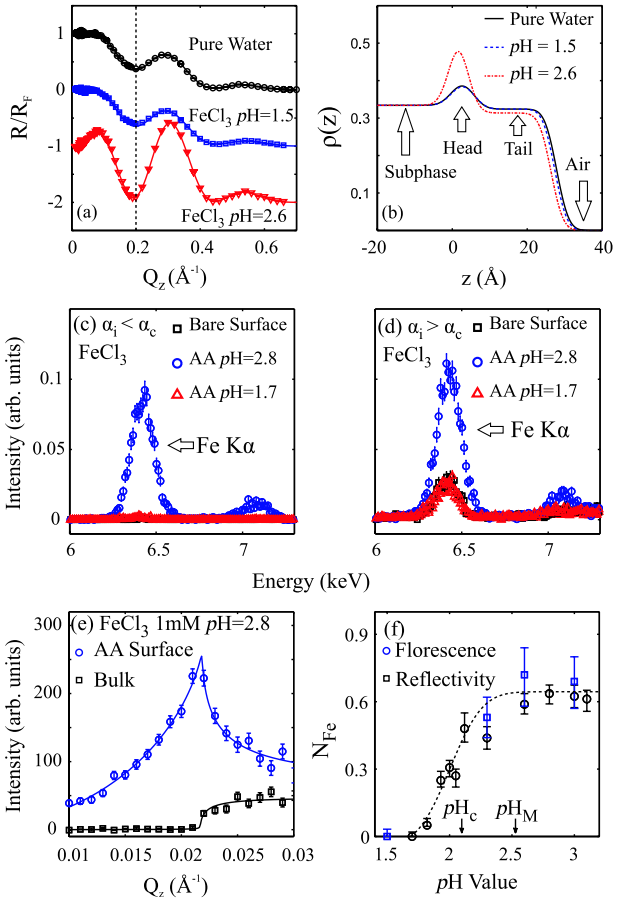

FIG. 2 (color online). (a) Normalized XR from monolayer on water and subphase at different pH. The symbols ○, □, and ▽ represent the experimental data of XR from the monolayer sitting on pure water, ferric chloride subphase of $p\mathrm{H} = 1.5$ and 2.6. Solid lines through these symbols are calculated reflectivities based on two-slab model (curves shifted vertically for clarity, vertical dash line indicates first minimum in curves). (b) ED profiles simulated by the best-fit parameters. (c) Fluorescence signal below critical angle (integrated over $Q_z = 0.01$–0.021 Å^{-1}). (d) Fluorescence signal above critical angle (integrated over $Q_z = 0.022$–0.03 Å^{-1}). (e) Integrated Fe emission line intensity over 6.2–6.6 keV with curve fit as function of Q_z. (f) pH dependence of iron accumulation at surface (dashed line is a guide to the eye).

Figures 2(c) and 2(d) show fluorescence spectra in the energy range of the Fe K_α (≈ 6.4 keV) and K_β (≈ 7.06 keV) below and above the critical angle (α_c) for total reflection, respectively. Below α_c, the fluorescence signal is dominated by the surface as the evanescent incident beam penetrates only to $\sim$60 Å, whereas above α_c the fluorescence signal has contributions from the bulk as well as from the enriched surface. For the bare surface without the monolayer and with the monolayer at $p\mathrm{H} = 1.7$, the signal below the critical angle is below the detection limit, indicating the absence of ion enrichment at the interface. However, in the presence of a monolayer at $p\mathrm{H} = 2.8$, there is evidence of strong binding. The analysis of the

spectra and its Q_z dependence [Fig. 2(e)] yields the number of bound iron ions at the interface [10,14]. Figure 2(f) shows the number of bound iron per molecule (N_{Fe}) at the interface as a function of pH, consistent with the isotherm measurements shown in Fig. 1. Furthermore, the maximum number of bound ions is ~0.6 per molecule, implying a higher accumulation of Fe^{3+} at the interface than that required for neutralizing a maximally charged interface (all carboxyl groups deprotonated). Similar measurements of La^{3+} solution at pH values 1.5, 2.7, and 5.0 yield 0, 0, and 0.3 La^{3+} ions per AA (data not shown). The specificity between the two ions is demonstrated not only in their pH dependence of binding, but also by the maximum bound ions per molecule. To further explore this excess of iron ions at the interface, we examined the fluorescence signal from the K_α emission lines of Cl ($\approx$ 2.62 keV) as shown in Fig. 3. The spectra show evidence for surface enrichment of the Cl coions with intense signal at pH values that correspond to excess iron binding to the AA.

To explain these observations, we employ the theoretical approach developed in Refs. [15,16], suitably generalized to account for the low surface charge density limit described in recent simulations [17]. We construct a free energy for the head group region of surface charges using four contributions, (1) the free energy of the diffuse layer of counterions and coions $\mathcal{F}_{\mathrm{PB}}$, (2) proton release and binding $\mathcal{F}_{\mathrm{prot}}$, (3) the mixing entropy of the different interfacial species $\mathcal{F}_{\mathrm{mix}}$, and (4) electrostatic correlations and ionic specific effects $\mathcal{F}_{\mathrm{corr}}$, and calculate the $\delta\pi_c$ (details are provided in the supplementary material [13]) as follows,

$$\delta\pi_c = \frac{\epsilon_r}{4\pi}\int_0^\infty dz\left(\frac{d\Phi}{dz}\right)^2 - k_BTf_{\mathrm{DC}}\gamma(f_b)\frac{l_B}{A_c^{3/2}}, \qquad (2)$$

where $\Phi(z)$ is the electric potential at distance z from the interface, $A_c \approx 20$ Å^2 is the molecular area, $l_B = \frac{e^2}{\epsilon_r k_B T} \approx$ 7.1 Å is the Bjerrum length, k_BT is the temperature, f_{DC} is the fraction of carboxyl groups that are charged (by releasing a proton), and f_b the fraction of headgroups with a bound trivalent counterion, which are obtained by minimizing the total free energy [16]. The positive function $\gamma(x)$ is quadratic in x and accounts for the electrostatic correlations among all the charged species including both condensed counterions and interfacial groups (the Stern layer; see supplementary information [13] for more details). Physically, Eq. (2) is a balance between the cost of compressing the diffuse layer of ions (repulsive) and the gain in electrostatic correlation energy arising from keeping charges as close as possible (attractive). The model does not have any fitting parameters, but it depends on external parameters, such as the carboxyl $pK_a = 5.1$ [18], ionic radius, and the free volume entropy of the bound counterion. The results for La^{3+} are shown in Fig. 1(c) and describe the experimental data satisfactorily, thus reassuring our assumption that the La^{3+} ion is, to a good approximation, well described as a classical ion [Fig. 4(a)]. By allowing reasonable variations of parameters such as ionic radii, free volume entropy, etc. (as described in the supplementary information [13]) within fairly liberal values (that should apply to Fe^{3+}), we obtain the dotted curves, thus showing that Fe^{3+} is completely dominated by ion-specific effects. In this way, La^{3+} and Fe^{3+} are representative of two extreme cases.

The first step towards understanding ion binding for Fe^{3+} is to evaluate the different ionic species in solution, which can be obtained from tabulated values of stability constants [18]. Detailed calculations (see supplementary information [13]) point to two limiting pH values, $p\mathrm{H}_M$ is the highest equilibrium pH value that a solution with Fe^{3+} and HCl can attain. At this pH, and below it, the bulk solution contains Fe^{3+}, $Fe(OH)_2^+$ and $Fe(OH)_2^+$, a result confirmed in recent experiments [19]. We note that there is also a considerable amount of $Fe(OH)_3$, but this complex is not soluble and therefore not observed in bulk solutions. The amount of $Fe(OH)_3$ decreases with decreasing pH down to a value $p\mathrm{H}_c$ where it becomes zero. A similar analysis for La^{3+} gives $p\mathrm{H}_c \sim 8$, with a bulk consisting of basically the free ion, thus reassuring our analysis for the $LaCl_3$ solutions.

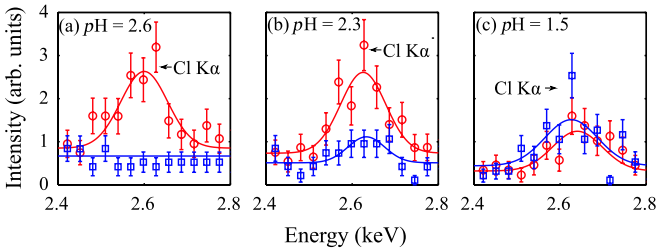

FIG. 3 (color online). Fluorescence spectrum showing chlorine characteristic emission line of subphase (a) $p\mathrm{H} = 2.6$, (b) $p\mathrm{H} = 2.3$, and (c) $p\mathrm{H} = 1.5$. The symbols ○ and □ represent the fluorescence with and without monolayer, respectively. The signals are integrated over $Q_z = 0.01$–0.021 Å^{-1}. Each point is obtained by binning three consecutive channels.

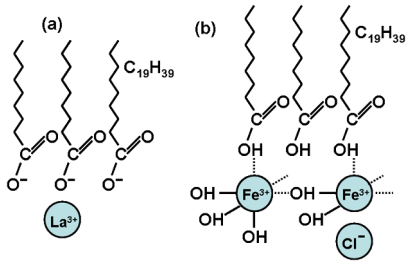

FIG. 4 (color online). Two scenarios of ion binding. (a) La^{3+} ions bind to charged surface by mainly electrostatic forces, and (b) bound $Fe(OH)_{3-z}^{z+}$ complexes to AA attract Cl^- coions.

The theoretical model shows that for $p\mathrm{H} < 3$ all carboxyl groups are protonated and the amphiphilic interface is charge neutral [Fig. 1(c)]. We propose that the accumulation of iron observed in Fig. 2 is the result of the insoluble component $Fe(OH)_3$ forming reversible covalent bonds, with several carboxyl headgroups as well as with other charged species [Fe^{3+}, $Fe(OH)^{2+}$, and $Fe(OH)^{2+}$], thus building a positively charged interface contiguous to the neutral amphiphile [Fig. 4(b)]. In this way, the ability of iron hydroxides to form covalent bonds with other hydroxyl groups induces a positive surface charge, which is externally regulated by pH. The presence of Cl ions for $p\mathrm{H} > p\mathrm{H}_c$, as demonstrated from spectroscopic x-ray measurements, provides support for this scenario.

The presence of Cl^- ions at the interface is remarkable, as, to our knowledge, this is the first direct evidence of coion accumulation at the interface. This phenomenon is known as charge reversal or inversion, and has also been observed experimentally in other systems involving trivalent ions [20–22]. However, the mechanism described here is different than in previous experiments and is not the result of counterion correlations (see [23] for a rigorous experimental realization). It is only possible specifically for Fe^{3+} and it is of much larger magnitude than that observed in other systems. In fact, the theoretical model applied to La^{3+} does predict charge inversion at $p\mathrm{H} > 4$, but with a much smaller magnitude, with Cl ion concentrations that are below experimental resolution, 0.1 per AA molecule.

In summary, using a combination of thermodynamic and x-ray scattering and spectroscopy methods, we present ion-specific effects and demonstrate that they can be quantitatively described by theoretical models. The results can be used to predict the effect of other trivalent and divalent ions such as in recent results for 1,2-Dimyristoyl-sn-glycero-3-phosphocholine (DMPC) monolayers [8] and for fatty acids [5], respectively, as briefly discussed in the supplementary material [13]. Our approach can also be expanded to crystal growths at biomimetic interfaces [24] and to ionic effects at cell membranes [25,26].

The work at the Ames Laboratory was supported by the Office of Basic Energy Sciences, U.S. Department of Energy under Contract No. DE-AC02-07CH11358. Use of the Advanced Photon Source was supported by the U. S. Department of Energy, Office of Science, Office of Basic Energy Sciences, under Contract No. DE-AC02-06CH11357.

[1] P. Koelsch *et al.*, Colloids Surf. A **303**, 110 (2007).
[2] V. Kaganer, H. Mohwald, and P. Dutta, Rev. Mod. Phys. **71**, 779 (1999).
[3] J. Kutscher, A. Gericke, and H. Huhnerfuss, Langmuir **12**, 1027 (1996).
[4] E. Le Calvez *et al.*, Langmuir **17**, 670 (2001).
[5] S. Kundu and D. Langevin, Colloids Surf. A **325**, 81 (2008).
[6] W. Bu *et al.*, Langmuir **25**, 1068 (2009).
[7] W. Bu, D. Vaknin, and A. Travesset, Phys. Rev. E **72**, 060501 (2005); Langmuir **22**, 5673 (2006).
[8] S. Kewalramani *et al.*, J. Phys. Chem. Lett. **1**, 489 (2010).
[9] D. Vaknin, in *Characterization of Materials*, edited by E. N. Kaufmann (John Wiley & Sons, New York, 2003), Vol. 2, pp. 1027–1047.
[10] W. Bu and D. Vaknin, J. Appl. Phys. **105**, 084911 (2009).
[11] D. Vaknin *et al.*, Biophys. J. **59**, 1325 (1991).
[12] D. Vaknin, P. Krüger, and M. Lösche, Phys. Rev. Lett. **90**, 178102 (2003).
[13] See supplemental material at http://link.aps.org/supplemental/10.1103/PhysRevLett.106.056102 for experimental details for x-ray scattering and analysis. Additionally, the theoretical model is built and used to account for isotherms of classical trivalent and divalent ions. Calculations of solubility of iron and its various complexes in water are also provided.
[14] W. B. Yun and J. M. Bloch, J. Appl. Phys. **68**, 1421 (1990).
[15] A. Travesset and D. Vaknin, Europhys. Lett. **74**, 181 (2006).
[16] A. Travesset and S. Vangaveti, J. Chem. Phys. **131**, 185102 (2009).
[17] C. Calero and J. Faraudo, J. Chem. Phys. **132**, 024704 (2010).
[18] A. E. Martell and R. M. Smith, *Critical Stability Constants* (Plenum, New York, 1977), Vols. 2, 3.
[19] A. Stefansson, K. H. Lemke, and T. M. Seward, in *Proceedings of the 15th International Conference on the Properties of Water and Steam*, edited by R. Span and I Weber (VDI, Düsseldorf, 2008), pp. 1–7.
[20] K. Besteman, M. A. G. Zevenbergen, and S. G. Lemay, Phys. Rev. E **72**, 061501 (2005).
[21] J. Pittler *et al.*, Phys. Rev. Lett. **97**, 046102 (2006).
[22] A. Martin-Molina, C. Rodriguez-Beas, and J. Faraudo, Phys. Rev. Lett. **104**, 168103 (2010).
[23] E. Wernersson, R. Kjellander, and J. Lyklema, J. Phys. Chem. C **114**, 1849 (2010).
[24] S. Kewalramani *et al.*, Langmuir **24**, 10 579 (2008).
[25] E. E. Kooijman *et al.*, Biophys. J. **96**, 2204 (2009).
[26] M. Broniatowski, M. Flasinski, P. Dynarowicz-Latka, and J. Majewski, J. Phys. Chem. B **114**, 9474 (2010).